Macroscopic Multifunctional Graphene-Based Hydrogels and Aerogels by a Metal Ion Induced Self-Assembly Process

Huai-Ping Cong,[†] Xiao-Chen Ren,[†] Ping Wang, and Shu-Hong Yu*

Division of Nanomaterials and Chemistry, Hefei National Laboratory for Physical Sciences at Microscale, Department of Chemistry, National Synchrotron Radiation Laboratory, University of Science and Technology of China, Hefei, Anhui 230026, People's Republic of China. [†]These two authors contributed equally to this work.

ABSTRACT

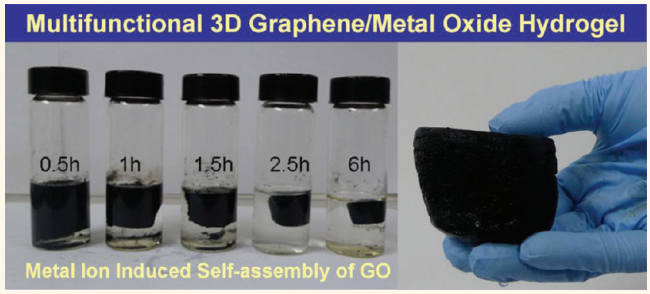

We report a one-step fabrication of macroscopic multifunctional graphene-based hydrogels with robust interconnected networks under the synergistic effects of the reduction of graphene oxide sheets by ferrous ions and *in situ* simultaneous deposition of nanoparticles on graphene sheets. The functional components, such as α-FeOOH nanorods and magnetic Fe_3O_4 nanoparticles, can be easily incorporated with graphene sheets to assemble macroscopic graphene monoliths just by control of pH value under mild conditions. Such functional graphene-based hydrogels exhibit excellent capability for removal of pollutants and, thus, could be used as promising adsorbents for water purification. The method presented here is proved to be versatile to induce macroscopic assembly of reduced graphene sheets with other functional metal oxides and thus to access a variety of graphene-based multifunctional nanocomposites in the form of macroscopic hydrogels or aerogels.

KEYWORDS: graphene · self-assembly · hydrogel · aerogel · α-FeOOH · magnetic Fe_3O_4 · nanocomposite

Self-assembly has been recognized as one of the most powerful techniques for integrating various nanostructured building blocks into macroscopic materials that can translate properties at the nanoscale into resulting macroscopic devices with hierarchical microstructures and novel functionalities.[1] Furthermore, the assembled superstructures are of novel collective physiochemical properties that are different from individual components and the bulk material, which enriches the species in the material fields and improves their capacities for practical applications.[2,3] Different interactions, such as dipole interactions, electrostatic attractions or repulsions, hydrophilic/hydrophobic interactions, and hydrogen bonding, have been involved in the driven self-assembly process.[4,5]

Graphene, a single layer of carbon atoms patterned in a hexagonal lattice, has attracted great attention all over the world for its potential applications in sensors,[6] catalysis,[7] energy-storage devices,[8] and environmental fields[9] due to the excellent mechanical, electronic, and thermal properties. Thus, graphene and its functionalized derivatives with unique two-dimensional (2D) structures can be well used as building blocks for self-assembly of functional carbon-based materials, such as 1D tube-in-tube nanostructures,[10] 2D graphene films,[11−13] and 3D graphene/polymer composites.[14−16]

Hydrogels and aerogels, the two typical kinds of 3D macroscopic assemblies, consisting of the microporous and mesoporous networks allowing access and diffusion of ions and molecules, possess attractive potentials in electrode materials, catalysis, and water treatment. Carbon nanotubes[17−19] and cellulose fibers[20] have been successfully used as building blocks for the assembly of carbon material gels. However, recent work on the preparation of 3D graphene gels and their functionalities is still limited. Among these reports, chemical or physical cross-linkers are used to prepare monolithic graphene architectures, such as organic binders via the sol−gel polymerization method,[21] DNA molecules,[22] ion linkages,[23,24] and ion coordination.[25] Otherwise,

* Address correspondence to shyu@ustc.edu.cn.

Received for review January 7, 2012 and accepted February 3, 2012.

Published online February 03, 2012
10.1021/nn300082k

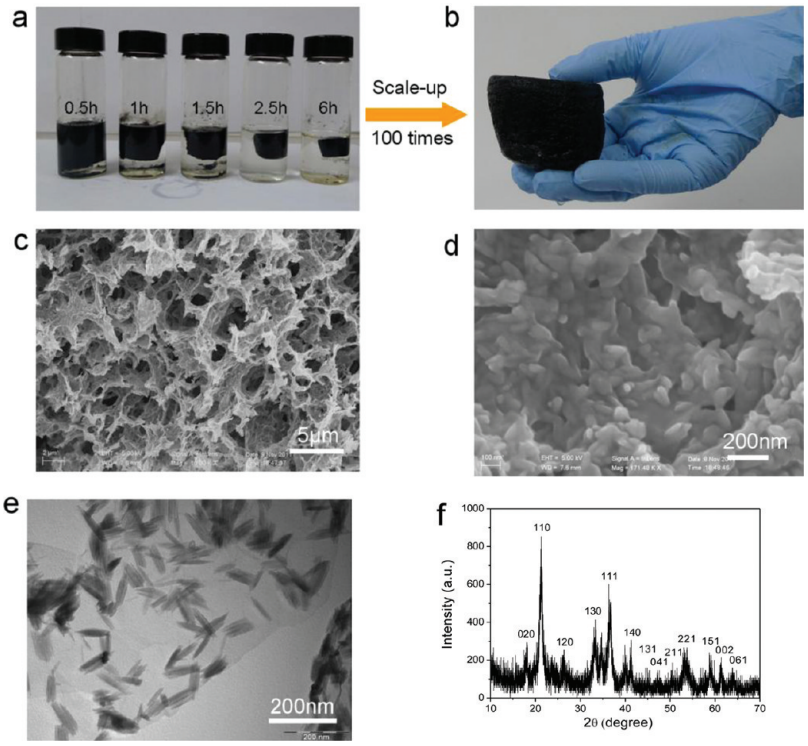

Figure 1. (a) Photographs of the time-dependent formation process of the hydrogels with 10 mL of GO (2 mg mL^{-1}) suspensions at pH 3 in the presence of 0.5 mmol of $FeSO_4$. The hydrogel was prepared in a cylindrical sampler vial with a volume of 25 mL. (b) Photograph of the scale-up synthesis of hydrogels by using 1000 mL of GO and 50 mmol of $FeSO_4$. (c and d) Low- and high-magnified SEM images. (e) TEM image of the microstructures of the freeze-dried graphene/FeOOH hydrogel. (f) XRD pattern of the graphene/FeOOH aerogel.

reducing mediums achieved by hydrothermal processes under high pressure[26] or using a large amount of reducing agents ($NaHSO_3$, Na_2S, vitamin C, sodium ascorbate, *etc.*)[27,28] have to be provided to satisfy the requirements of the assembly of macroscopic graphene-based hydrogels.

An abundance of oxygen-containing functional groups on graphene oxide (GO) sheets make it soluble and easily processable, which leads to the growth of new types of graphene-based materials, that is, decorating the 2D graphene sheets with nanoparticles.[29−31] However, until now, very few reports were focused on the assembly of 3D graphene-based hydrogels with deposited nanoparticles. Recently, Chen *et al.* reported the capture of preprepared magnetic nanoparticles into 3D graphene networks under the assistance of reducing agent ($NaHSO_3$, Na_2S, vitamin C, HI, and hydroquinone).[27,32] Thus, there is still a great challenge to develop facile methods for the preparation of functionalized graphene monolithic hydrogels with integrated functionalities and the advantages of both graphene sheets and nanoparticles.

In this article, we demonstrate a facile one-step approach for fabrication of macroscopic graphene/iron oxide hydrogels with 3D interconnected networks under the synergistic effects of the self-assembly of graphene oxide sheets and *in situ* simultaneous deposition of metal oxide nanoparticles such as α-FeOOH nanorods and magnetic Fe_3O_4 nanoparticles on graphene sheets induced by ferrous ions as a reducing agent to reduce the graphene oxide sheets under mild conditions. Herein, the compositions of graphene hydrogels can be easily changed via adjusting the pH value of the initial GO suspension with other conditions constant. Interestingly, when burning the oil-saturated graphene/α-FeOOH superhydrophobic aerogel directly, a 3D hematite α-Fe_2O_3 monolith with porous microstructures can be prepared. Furthermore, the facilely separable and low-cost graphene/metal oxide hydrogels and aerogels exhibit excellent capability for removal of heavy metal ions and oils from water, thus can be potential candidates for efficient adsorbents in water purification or other applications.

RESULTS AND DISCUSSION

In a typical synthesis, a mixture of 10 mL of GO suspension (2 mg mL^{-1}) and $FeSO_4$ (0.5 mmol) was undisturbedly sealed in an oil bath at 90 °C. As shown in the time-dependent photographs of Figure 1a, after 0.5 h, the black, reduced GO sheets were uniformly dispersed in water, without obviously aggregated sheets, but slightly floating from the bottom of vessel. With prolonging the reaction time (*e.g.*, 1 h, 1.5 h), the assembled graphene monolith floated toward the top of the water surface. With prolonging the reaction, the black aggregate further shrunk, as a result of decreasing the diameter of the columnar hydrogel. After 6 h, a

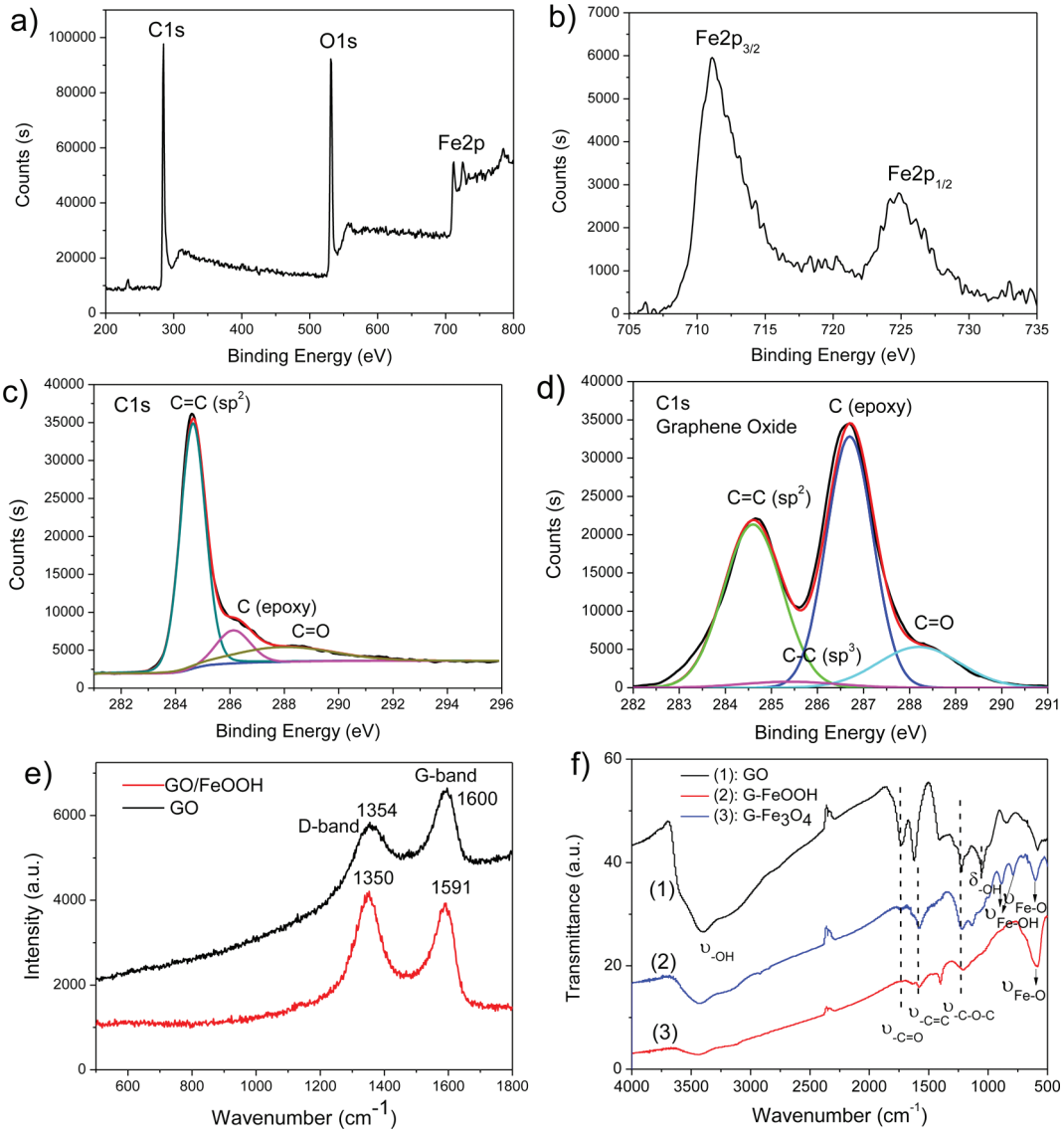

Figure 2. XPS spectra of (a) the graphene/FeOOH aerogels; (b) core-level Fe2p; (c) core-level C1s of the graphene/FeOOH hydrogel prepared with 10 mL of GO (2 mg mL^{-1}) suspensions at pH 3 in the presence of 0.5 mmol of $FeSO_4$; (d) core-level C1s of GO. (e) Raman spectra of the graphene/FeOOH aerogel sample in (a). (f) FT-IR spectra of (1) GO; (2) the graphene/FeOOH aerogel; (3) graphene/Fe_3O_4 aerogel dried from the hydrogel prepared with 10 mL of GO (2 mg mL^{-1}) suspensions at pH 11 in the presence of 0.5 mmol of $FeSO_4$. The hydrogel was prepared in a cylindrical sampler vial with a volume of 25 mL.

well-defined black hydrogel in a columnar shape with an unchanged size of 10 mm in diameter and 7 mm in height formed. Interestingly, except for the integrated cylinder, there were no separated graphene sheets elsewhere, and the transparent solution was left in the vessel.

One key advantage of the present synthetic route is that it is easy to scale up, as shown in the photograph in Figure 1b, which presents the successful self-assembly of 1000 mL of GO suspension into the integrated hydrogel by just using a large reaction vessel of 1500 mL without changing other parameters, such as concentrations, temperature, and reaction time (Supporting Information, Figure S1). As demonstrated previously for the synthesis of 3D hydrogels of graphene oxide based on a hydrothermal process using metal ions and glucose as mediators,[23,24,26] a metal ion mediated gelation process,[25] and adding reducing agents (Na_2S, vitamin C, HI, and hydroquinone),[27,32] the larger scale-up synthesis of such hydrogels in the present case can be achieved by using the proper reaction vessel with a different volume or shape. The as-prepared graphene hydrogel containing about 95.8 wt % water exhibited a well-defined and interconnected 3D network microstructure with uniformly dispersed pores of several micrometers in size, as shown from the SEM image in Figure 1c. More interestingly, a large number of nanoparticles homogenously enwrapped in the graphene sheets were found by a magnified SEM image (Figure 1d). Furthermore, the TEM image of Figure 1e shows that all of the rod-like nanoparticles with a size of about 60 nm were

anchored onto the thin graphene sheets; no particles that were disassociated from the graphene sheets were observed.

The XRD pattern in Figure 1f illuminated the compositions of the 3D graphene aerogel. All the diffraction peaks can be assigned to a pure orthorhombic phase α-FeOOH (JCPDS No. 29-0713). The presence of the elements C, O, and Fe with high contents in the graphene aerogel was evidenced by the photoelectron lines of the wide-scan XPS spectrum in Figure 2a at 285, 532, and 711 eV, attributed to C1s, O1s, and Fe2p, respectively. In the high-resolution Fe2p XPS spectrum in Figure 2b, the peaks of $Fe2p_{3/2}$ and $Fe2p_{1/2}$ at 711.1 and 724.7 eV were the characteristic positions of α-FeOOH,[33] indicating the existence of α-FeOOH nanorods in the graphene support. In the formation process of the graphene/α-FeOOH hydrogel, the initial GO was reduced to graphene by ferrous ions, confirmed by significantly improving the intensity of sp^2 C−C bonds of graphene at 284.6 eV and decreasing the oxygen-containing carbon (epoxy C−O at 286.5 eV, carbonyl C═O at 287.9 eV, and carboxyl O═C−O at 289.0 eV),[34] as analyzed from the deconvoluted C1s spectra of the as-prepared aerogel and GO in Figure 2c and d. In the Raman spectra of GO and graphene/α-FeOOH aerogel, as shown in Figure 2e, the intensity ratio of the well-documented D band and G band of graphene in the aerogel was enhanced after reduction compared with that for GO, indicating the improvement of the disordered graphene sheets.[35] Furthermore, the peak shifts of two bands to 1350 and 1591 cm^{-1} revealed the charge transfer between graphene sheets and α-FeOOH nanorods.[36] In comparison with the FT-IR spectra of GO and the graphene/α-FeOOH aerogel in Figure 2f, the absorption bands of carbonyl at 1730 cm^{-1} and epoxy C−O at 1225 cm^{-1} of GO were obviously decreased, indicating the effective reduction of graphene sheets. Meanwhile, two bands at 892 and 783 cm^{-1} in the product were the characteristic bending vibrations of Fe-OH.[37] Thus, from the above analyses, it was reasonable to conclude that our hydrogels were formed by coassembly of graphene sheets and α-FeOOH nanorods.

The rheological measurements in Figure 3a further revealed the structure and property of the graphene/α-FeOOH hydrogel. As a function of angular frequency (1−100 rad·s^{-1}), the independent storage modulus (G') and slightly sensitive loss modulus (G'') to frequency were characteristics of the hydrogel materials. Moreover, G' was almost 1 order of magnitude larger than G'' over the whole tested range, indicating an elastic rather than viscous response of the composite hydrogel with the permanent cross-linked network. The G' value of 50 kPa at 10 rad·s^{-1} was 1 to 2 orders of magnitude higher than the conventional self-assembled hydrogels.[38,39] Moreover, the good thermal stability of such a hydrogel was demonstrated by the

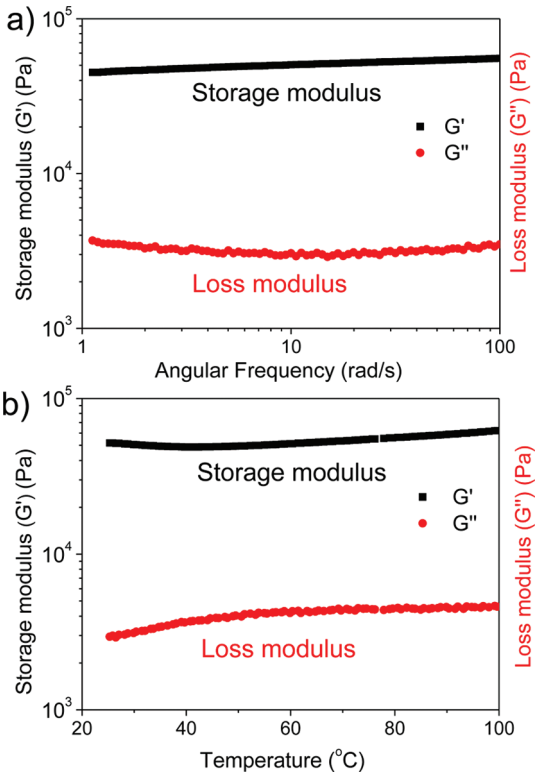

Figure 3. (a) Dynamic rheological behavior of the graphene/FeOOH hydrogel prepared with 10 mL of a GO (2 mg mL^{-1}) suspension at pH 3 in the presence of 0.5 mmol of $FeSO_4$. The reaction was performed in a cylindrical sampler vial with a volume of 25 mL. (b) Storage (G') and loss (G'') modulus as a function of temperature.

invariable values of G' and G'' for the entire temperature range (25−100 °C), due to the strong interconnected networks, as shown in Figure 3b. The compression−strain curve of the graphene/FeOOH hydrogel exhibited a linear stage at low strains (<10%), a gradually increasing stage up to 60%, followed by the densification stage, behaving like an "elastic-plastic" under compression (Supporting Information, Figure S2).[26] The elastic modulus and yield stress of the free-standing graphene hydrogel were calculated to be about 0.1 MPa and 23.6 kPa, respectively. The inset in Figure S2 shows a 3D hydrogel cylinder supporting the weight of 100 g, as a proof of its good mechanical property.

Furthermore, it was found that the properties of the graphene/α-FeOOH hydrogel largely depended on the amount of reducing agent Fe(II). A higher concentration of $FeSO_4$ in the GO suspension resulted in the well-defined 3D network-like graphene hydrogel decorated with more α-FeOOH nanorods, as clearly observed from the SEM and TEM images (Figure 4a−c). However, if the amount was lower than 0.0625 mmol, a few nanoparticles appeared on the sheets, and the pores with a size of tens of micrometers led to a larger 3D gel cylinder, indicating the weak interaction within the network of the hydrogel (Figure 4d−f). When a series of

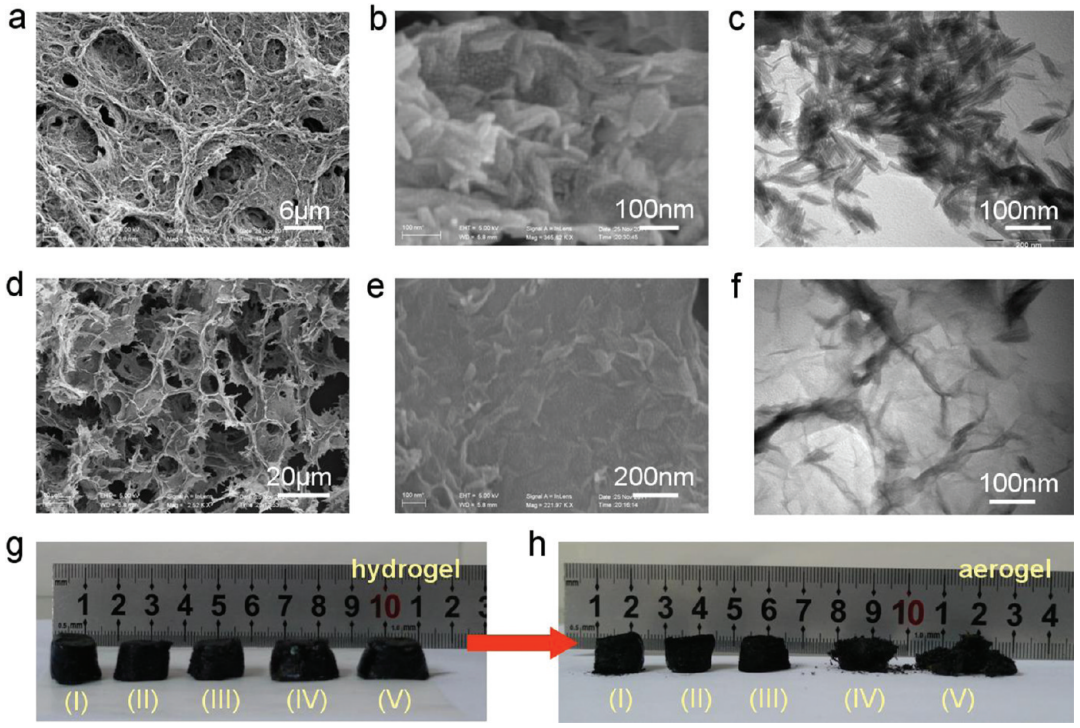

Figure 4. SEM images with different magnifications of the graphene/FeOOH aerogels dried from the hydrogels prepared with 10 mL of a GO (2 mg mL^{-1}) suspension at pH 3, using different amounts of $FeSO_4$: (a–c) 1 mmol; (d–f) 0.0625 mmol. Photographs of the graphene/FeOOH hydrogels (g) and corresponding aerogels (h) dried from the hydrogels prepared using different amounts of $FeSO_4$. The amount of $FeSO_4$ used for preparation of the samples (I)–(V) shown in (g) and (h) is 1, 0.5, 0.25, 0.125, and 0.0625 mmol, respectively. The hydrogel was prepared in a cylindrical sampler vial with a volume of 25 mL.

graphene hydrogels (samples I–V listed in Table 1) prepared by adding different amounts of $FeSO_4$ (from 1 to 0.0625 mmol) were freeze-dried to aerogels, the last two samples collapsed (Figure 4g and h). Further characterization of the powdery aerogel (sample V) prepared with the lowest amount of reducing agent (0.0625 mmol) revealed that GO was still evolving to reduced graphene oxide sheets, but was not so highly reduced, which can be explained by the intensity ratio of the D band and G band in the Raman spectra and the content of oxygen-containing carbon in deconvoluted C1s XPS spectra (Supporting Information, Figure S3). Thus, the low degree of reduced GO in the sample was the reason for the collapse of the last two aerogels with weak cross-linking ability.

Interestingly, the compositions of the as-prepared graphene hydrogels were significantly affected by the pH values of the initial GO suspension adjusted with ammonia, as revealed from a series of XRD patterns of the pH-controlled samples (pH 3–10) (Supporting Information, Figure S4). At low pH (3–6), the nanoparticles deposited on the graphene sheets were α-FeOOH. While using NH_4OH to change the pH value of the GO suspension from 7 to 10, the α-FeOOH phase was dominant in the products, and the diffraction peaks for the $Fe(OH)_3$ phase marked with asterisks appeared simultaneously (Figure S4). On further increasing the pH value of the initial GO suspension to 11, the magnetic 3D graphene hydrogel can be fabricated,

TABLE 1. Experimental Parameters and Composition Analyses for the Samples Prepared at pH 3

sample[a]	$n_{FeSO4(initial)}$ (mmol)	$m_{hydrogel}$ (g)	$m_{aerogel}$ (g)	water content (%)	$m_{FeOOH}/m_{aerogel}$ (%)[b]
I	1	1.175	0.056	95.2	75.6
II	0.5	1.174	0.049	95.8	59.8
III	0.25	1.188	0.032	97.3	46.2
IV	0.125	1.699	0.022	98.7	22.1
V	0.0625	1.622	0.019	99.0	10.5

[a] The initial amount of GO in the experiments was 2 mg/mL (10 mL). [b] The values were analyzed by inductively coupled plasma atomic emission spectrometry (ICP-AES). The hydrogel was prepared in a cylindrical sampler vial with a volume of 25 mL.

which was shown by the attraction to a magnet in the photograph in Figure 5a. The SEM image in Figure 5b revealed the interconnected network with the porous structure of the magnetic hydrogel. From the high-magnified SEM image and TEM image of Figure 5c,d, a large number of nanoparticles with a size of 30 nm were uniformly decorated onto the thin graphene sheets, and no free nanoparticles from the sheet supports can be found. All of the diffraction peaks were indexed to the magnetic Fe_3O_4 phase (JCPDS No.75-0033), as shown by the XRD pattern of the magnetic hydrogel in Figure 5e. The Raman spectrum of the freeze-dried magnetic aerogel in Figure 5f showed a large value of the intensity ratio of the D

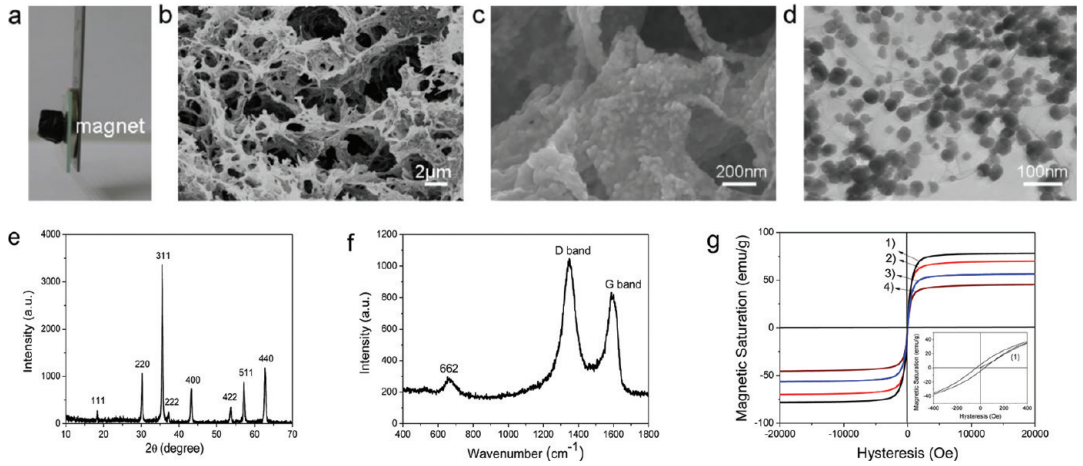

Figure 5. (a) Photograph of the magnetic property of the hydrogel under a magnet. SEM image with low (b) and high (c) magnification of the interior microstructures of the freeze-dried graphene/Fe_3O_4 hydrogel prepared in the presence of 0.5 mmol of $FeSO_4$ at pH 11. (d) TEM image of the microstructures of the hydrogel after sonication. (e) XRD pattern. (f) Raman spectrum of the magnetic aerogel. (g) Room-temperature hysteresis curves of the magnetic aerogels prepared using different amounts of $FeSO_4$ at pH 11. Samples 1−4 were prepared using 1, 0.5, 025, and 0.125 mmol of $FeSO_4$, respectively.

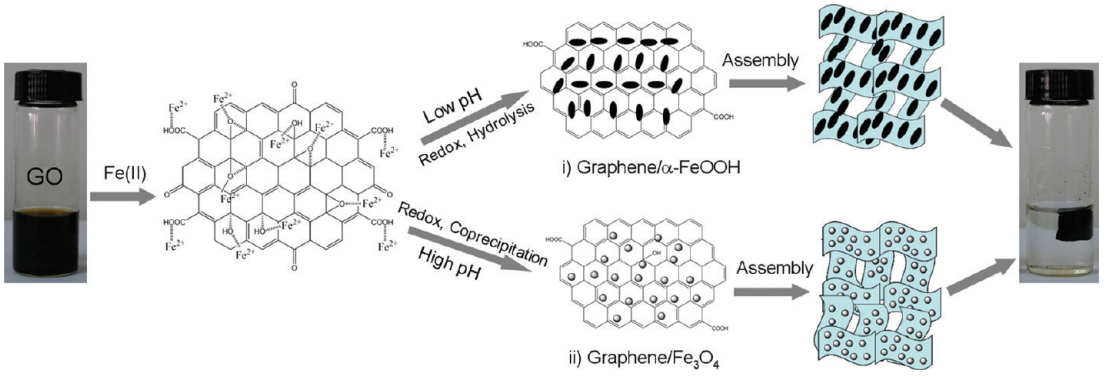

Scheme 1. Schematic illustration of the formation mechanism of the graphene/iron oxide hydrogels.

band and G band, indicative of the high degree of reduction of the graphene sheets, as well as a band at 662 cm^{-1} associated with the A_{1g} mode of Fe_3O_4. The effective reduction of GO to graphene sheets and the formation of Fe_3O_4 in the magnetic hydrogel were proved by the information in the FT-IR spectrum in Figure 2f.

To investigate the magnetic properties, a series of magnetic hysteresis curves for magnetic graphene aerogels with different amounts of Fe_3O_4 nanoparticles were recorded at room temperature, shown in Figure 5g. The sample showed ferromagnetic properties, revealed by the magnified plot in the inset: the coercive force of 38.6 Oe and a remanent magnetization of 4.8 emu·g^{-1}. The saturation magnetization (M_s) of the magnetic aerogels was improved from 45.2 to 80.3 emu·g^{-1} with the increase of the amount of embedded Fe_3O_4 nanoparticles, comparable to the bulk magnetite Fe_3O_4 (92 emu·g^{-1}),[40] which was much higher than the reported 3.4 emu·g^{-1} for graphene/Fe_3O_4, despite the similar presence of abundant graphene in our tested samples.[32] Thus, it can be deduced that such strong magnetic signals at small applied magnetic fields of the as-obtained novel functional graphene hygrogels are desirable for practical applications.

The formation mechanism of the novel graphene/iron oxide hydrogels is illustrated in Scheme 1. The ferrous ions Fe^{2+} tended to diffuse toward the GO sheets by electrostatic interactions, which were then oxidized into ferric ions Fe^{3+} effectively by the oxygen-containing functional groups on the GO surface.[41] At low pH value, the resultant α-FeOOH nanorods were *in situ* deposited on the reduced GO surfaces simultaneously by hydrolysis of Fe^{3+} ions. However, when the pH value of the initial GO suspension was increased with NH_4OH, the oxidized Fe^{3+} ions and Fe^{2+} ions coprecipitated into Fe_3O_4, similar to the formation of graphene sheets decorated with nanoparticles, as reported previously.[29,30,42] Meanwhile, the reduced graphene oxide sheets anchored with nanoparticles were simultaneously self-assembled into the 3D hydrogel with interconnected networks driven by combined hydrophobic and $\pi-\pi$ stacking interactions, due to the decrease of oxygenated groups on the graphene sheets. Furthermore, the deposited nanoparticles on

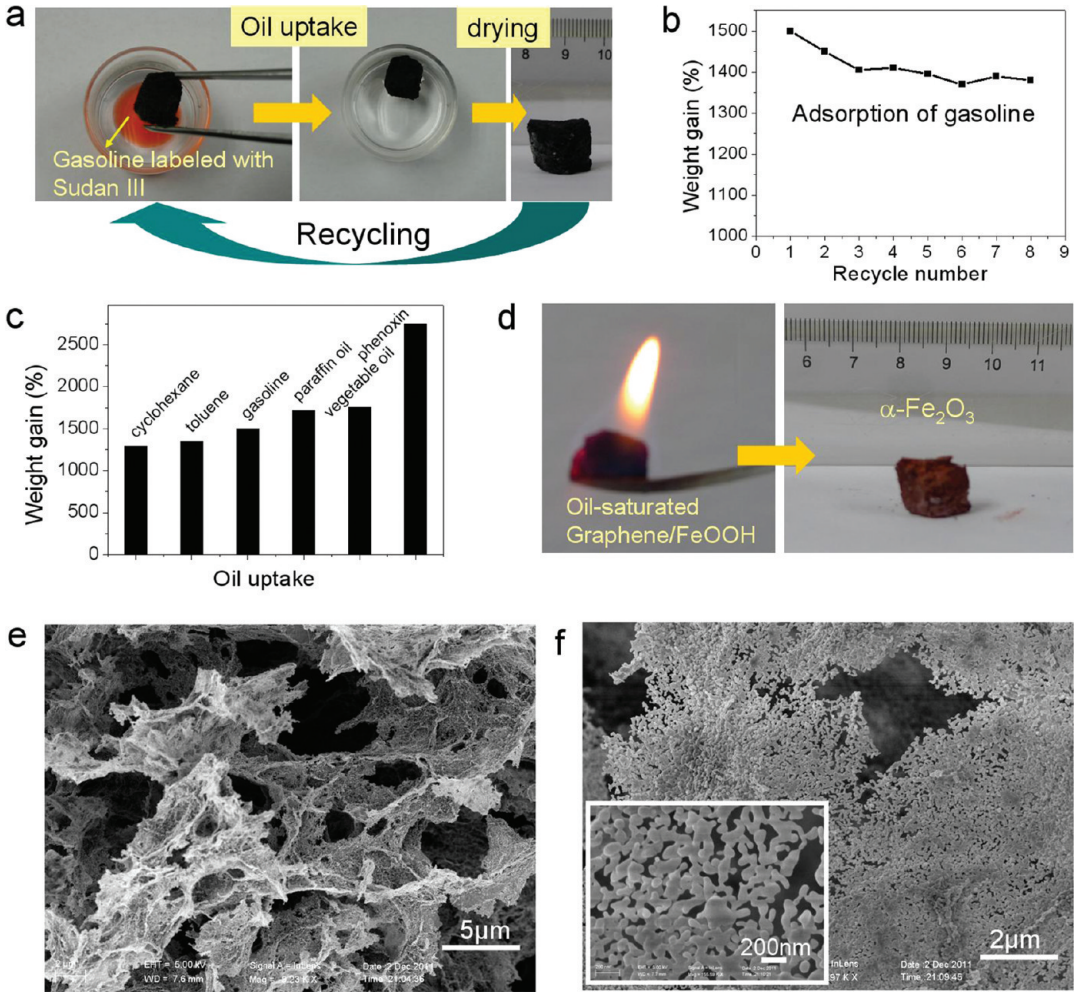

Figure 6. (a) Photographs showing the process of the graphene/α-FeOOH aerogel adsorbing gasoline. The graphene/α-FeOOH aerogel was dried from the hydrogel prepared with a 10 mL of GO (2 mg mL^{-1}) suspension at pH 3 in the presence of 0.5 mmol of $FeSO_4$. The gasoline was labeled with Sudan III for clear presentation. (b) Regeneration capacity of the aerogels for adsorbing gasoline. Gasoline can be removed by putting the aerogel in the oven at 100 °C for recycled use. (c) Adsorption capacities of the aerogels for a range of organic solvents and oils in terms of its weight gain. (d) Photographs of burning the oil-saturated graphene/α-FeOOH aerogel. (e, f) SEM images of the three-dimensional microstructures of the product α-Fe_2O_3 by burning the oil-saturated graphene/α-FeOOH aerogel.

the graphene sheets facilitated stabilizing such novel graphene hydrogels, which served as the space to effectively avoid aggregation of the graphene sheets during the reduction process.[23] The important role of the nanoparticles in such a graphene hydrogel system was proved by etching a graphene/α-FeOOH hydrogel with HCl to dissolve α-FeOOH nanorods (Supporting Information, Figure S5). The 3D network structures were broken down due to the severe reaggregation of the graphene sheets, as revealed from the photograph of the loose graphene block and cross-sectioned SEM image. Importantly, in addition to ferrous ions, other metal ions, such as Mn (II) and Ce(III), can also induce the assembly of the reduced GO sheets, forming macroscopic graphene/Mn_2O_3 and graphene/CeO_2 hydrogels by this simple one-step method (Supporting Information, Figure S6), showing that this is a general approach for fabrication of graphene/metal oxide hydrogels.

Another advantage of the novel graphene/α-FeOOH aerogel was that it was superhydrophobic and porous to adsorb oils and nonpolar organic solvents without the suctioning of water, which could find practical applications as a suction skimmer in marine oil-spill recovery.[43] The photographs in Figure 6a show the fast process of the aerogel selectively absorbing a layer of gasoline labeled with Sudan III dye on the water surface under superhydrophobic and capillary effects. Furthermore, it was found that the aerogel had an excellent regeneration capacity, an important index of a promising adsorbent. As shown in Figure 6b, the graphene/α-FeOOH aerogel adsorbent maintained a high adsorption capacity (92% of the first maximum) after eight gasoline-absorbing and drying recycles, due to the robust interconnected network and stable porous structure. To measure the adsorption capability of the aerogels, they were sucked into a wide range of

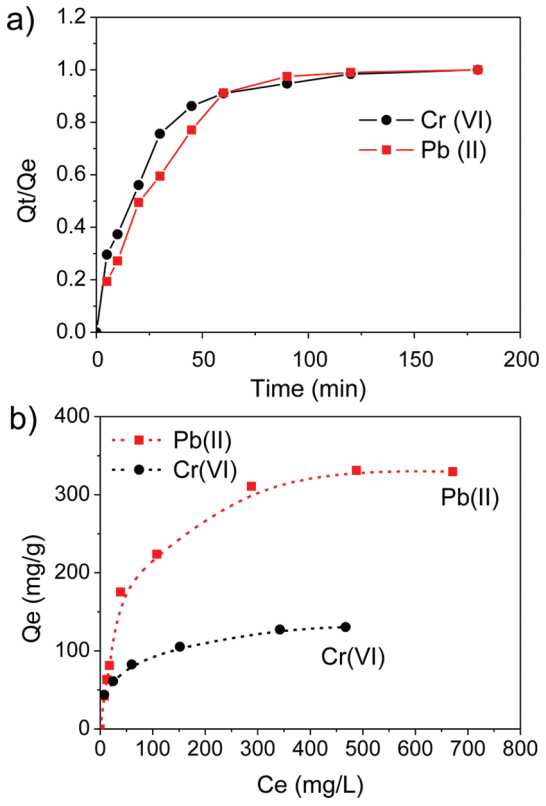

Figure 7. (a) Adsorption rate plots. (b) Adsorption isotherms of Cr(VI) and Pb(II) on the graphene/FeOOH hydrogel at room temperature, which was prepared with 10 mL of a GO (2 mg mL^{-1}) suspension at pH 3 in the presence of 0.5 mmol of $FeSO_4$. Q_t and Q_e represented the adsorption capacity at time t and equilibrium capacity ($mg \cdot g^{-1}$), respectively. C_e was the equilibrium solute concentration ($mg \cdot L^{-1}$).

nonpolar organic solvents and oils and weighed. As shown in Figure 6c, the maximum uptake capacity was 27 times its weight, fluctuating with the densities of the solvents. The unusual superwetting and high selectivity of our graphene/α-FeOOH aerogel for adsorbing oils were attributed to the hydrophobic $\pi-\pi$ stacking of the reduced graphene and abundant inorganic nanoparticles on the graphene sheets, which dramatically increased the surface roughness of the adsorbent.[44,45]

Interestingly, when burning the black oil-saturated graphene/α-FeOOH aerogel directly, a red cylinder was obtained (Figure 6d), which was the pure hematite α-Fe_2O_3 phase, revealed by the diffraction peaks of the XRD pattern (Supporting Information, Figure S7). The novel microstructures of such a burned α-Fe_2O_3 architecture were revealed by the different magnifications of the SEM images in Figure 6e,f. To some extent, the product remained as an interconnected porous network with thin sheets of tens of micrometers in size. However, the intensity became weaker than that of the graphene/α-FeOOH aerogel before burning. The magnified SEM image clearly showed that the porous sheets consisted of nanoparticles when the graphene sheets were burned out (Figure 6f). Importantly, no isolated particles were found elsewhere but were interconnected with each other to form a thin but free-standing sheet, as shown in the SEM image in Figure 6e. Therefore, our superhydrophobic graphene/α-FeOOH aerogel can be used as a novel and simple precursor to effectively fabricate functional metal oxide monoliths with interesting 3D microstructures.

In addition, given the serious worldwide water pollution caused by heavy ions, recent reports on metal oxides and carbon-based nanoadsorbents have shown excellent activities for purifying polluted water.[9,40,46,47] Herein, the economical self-assembled 3D graphene/α-FeOOH hydrogel fabricated under mild conditions could act as a promising candidate for removal of pollutants, inspired by its advantage of its robust interconnected networks, and, thus, its easy separation from water. Figure 7a shows the adsorption rates of heavy ions Cr(VI) and Pb(II), highly toxic pollutants in water resources, to test the adsorption kinetics of our macroscopic adsorbents at room temperature. When the initial concentration of Cr(VI) or Pb(II) was 100 mg/L, about 60% of the heavy ions were adsorbed from the water within 20 min, and after 90 min, the adsorption was in an equilibrium state.

The adsorption behaviors of the graphene/α-FeOOH hydrogel absorbents for Cr(VI) or Pb(II) were reflected by adsorption isotherms in Figure 7b, which well fitted with the Langmuir isotherm model.[48] The calculated maximum adsorption capacities for Cr(VI) and Pb(II) were 139.2 and 373.8 $mg \cdot g^{-1}$, respectively, which are much higher than mesoporous γ-Fe_2O_3 and active carbon for Cr(VI) (15.6[49] and 69 $mg \cdot g^{-1}$,[50] respectively) and exfoliated graphene sheets and chrysanthemum-like and commercial bulk α-FeOOH for Pb(II) (40,[51] 103.0, and 1.0 $mg \cdot g^{-1}$,[47] respectively) and slightly lower than our reported free-standing carbonaceous nanofiber membranes for Cr(VI) (173−221 $mg \cdot g^{-1}$) and Pb(II) (310−423 $mg \cdot g^{-1}$).[46] However, most of the above adsorption results in the literatures were recorded at optimal pH values, which had a significant effect on the adsorption capacities of the adsorbents for the pollutant uptake.[9] Thus, it was more indicative to estimate the potential capability of our graphene/FeOOH hydrogel for heavy-ion removal in practical water purification, as it was measured directly, without the need for any pH adjustment. The strong adsorption capacity of the hydrogel with graphene sheets and α-FeOOH nanorods possibly arose from the synergistic effects of the static electrical attraction, ion exchange, and surface complexation between metal oxyhydroxides and heavy ions, as well as the remaining oxygen-containing groups of the graphene sheets and heavy ions.[52,53]

CONCLUSION

In summary, we report that novel self-assembled graphene/α-FeOOH and magnetic graphene/Fe_3O_4 hydrogels with robust interconnected 3D networks can be fabricated on a large scale, effectively induced by Fe(II) ions at different pH values via a simple one-step method under mild conditions. Interestingly, the pure free-standing α-Fe_2O_3 monolith with elegant microstructures composed of interconnected nanorods can be easily prepared by burning the oil-saturated graphene/α-FeOOH aerogel directly. The multifunctional graphene-based hydrogels and aerogels are not only composition-flexible but the ideal candidates as adsorbents with high adsorption capacity for removal of heavy ions and oils in industrial water purification. The versatile method presented here can be extended to induce the assembly of graphene sheets and other functional metal oxides *via* one step into different macroscopic monoliths with multifunctionalities for different applications.

METHODS

Self-Assembly of Graphene/FeOOH and Graphene/Fe_3O_4 Hydrogels. GO was prepared from natural graphite powders according to Hummers' method.[54] In a typical synthesis, a certain amount of $FeSO_4$ (1−0.0625 mmol) was quickly added into 10 mL of a 2 mg mL^{-1} GO aqueous suspension stored in a 25 mL cylindrical sampler vial. The pH value of the GO suspension was adjusted with ammonia from 3 to 11 to investigate the influences of the pH value on the synthesis of graphene/FeOOH and graphene/Fe_3O_4. Then, the reaction vessel was placed in an oil bath for 6 h at 90 °C without stirring. Finally, the 3D black monolith was taken out, washed with distilled water, and freeze-dried into an aerogel for further use.

Characterizations. The microstructures of the aerogel were characterized by scanning electron microscope (SEM) images, taken with a Zeiss Supra 40 scanning electron microscope at an acceleration voltage of 5 kV, and transmission electron microscope (TEM) images by a JEOL-2010 microscope at an acceleration voltage of 200 kV. For revealing the compositions of the hydrogels, X-ray diffraction (XRD) analysis was performed on a Japan Rigaku DMax-γa rotation anode X-ray diffractometer equipped with graphite-monochromatized Cu Kα radiation (λ = 0.15418 nm). The X-ray photoelectron spectrum (XPS) was tested on an ESCALab MKII X-ray photoelectron spectrometer using a Mg Ka radiation exciting source. Raman spectra were conducted on a confocal laser micro Raman spectrometer (LABRAM-HR, JY Co.). FTIR spectra were recorded on a Bruker Vector-22 FTIR spectrometer from 4000 to 400 cm^{-1} at room temperature. The magnetic properties of the samples were investigated using a superconducting quantum interface device (SQUID) magnetometer (Quantum Design MPMS XL). The inductively coupled plasma atomic emission spectrometry (ICP-AES) measurements were carried out using an Atomscan Advantage spectrometer (Thermo Ash Jarrell Corporation, USA). UV−vis spectra were recorded on a Shimadzu UV-240 spectrophotometer scanning from 400 to 800 nm at room temperature.

Rheological and Mechanical Measurements. The dynamic rheological measurements of the as-prepared hydrogels were performed by a TA-AR2000 rheometer with parallel-plate geometry (CP25-2) at 25 °C. Dynamic frequency sweep experiments were measured from 1 to 100 rad/s with the distance of two plates fixed at 1 mm and the oscillatory strain at 0.2%. Temperature sweep experiments from 25 to 100 °C were investigated at a heating rate of 5 °C/min. To prevent evaporation of water, the samples were covered by a thin layer of mineral oil. The compressive stress−strain test for the cylindrical hydrogel was measured by using Instron 5565A equipped with two flat-surface compression stages and 500 N load cells.

Oil-Uptake Experiments. The oil-adsorbent capacity of the aerogels was determined by weight measurements. The weighed samples were put into different kinds of oils and taken out by tweezers after 1 min. After removing the oil on the surface of the samples with filter paper, the samples were weighed again. The oil adsorption values were calculated from the differences of mass. The regeneration of adsorbent capacity was investigated in the same way after the oil-saturated samples were dried in an oven at 100 °C for 30 min.

Adsorption Isotherm Experiments for Heavy Ions. At room temperature, graphene/FeOOH hydrogels equivalent to 10 mg of aerogels were added into 50 mL of heavy ion-containing solution of different concentrations. The temperature was maintained at 25 °C. After 12 h to reach complete adsorption equilibrium, the remaining concentrations of Cr(VI) and Pb(II) were measured by the reported colorimetric method[55] via UV−vis spectra and ICP-AES technique, respectively.

Conflict of Interest: The authors declare no competing financial interest.

Acknowledgment. This work is supported by the National Basic Research Program of China (2010CB934700), the National Natural Science Foundation of China (Nos. 21001099, 91022032, 21061160492, J1030412), the International Science & Technology Cooperation Program of China (2010DFA41170), and the Principal Investigator Award by the National Synchrotron Radiation Laboratory at USTC. H.P.C. thanks the Fundamental Research Funds for the Central Universities, China Postdoctoral Science Foundation (20110490086), and the Foundation for the Author of Excellent Doctoral Dissertation of the Chinese Academy of Sciences (CAS).

Supporting Information Available: Photographs of the graphene/FeOOH hydrogel, the compression−strain curve of the graphene/FeOOH hydrogel, Raman and XPS spectra of the samples, SEM images, and XRD pattern of the samples. This material is available free of charge *via* the Internet at http://pubs.acs.org.

REFERENCES AND NOTES

1. Vanmaekelbergh, D. Self-Assembly of Colloidal Nanocrystals as Route to Novel Classes of Nanostructured Materials. *Nano Today* **2011**, *6*, 419–437.
2. Mann, S. Self-Assembly and Transformation of Hybrid Nano-Objects and Nanostructures under Equilibrium and Non-Equilibrium Conditions. *Nat. Mater.* **2009**, *8*, 781–792.
3. Gao, Y.; Tang, Z. Design and Application of Inorganic Nanoparticle Superstructures: Current Status and Future Challenges. *Small* **2011**, *7*, 2133–2146.
4. Xia, Y.; Nguyen, T. D.; Yang, M.; Lee, B.; Santos, A.; Podsiadlo, P.; Tang, Z.; Glotzer, S. C.; Kotov, N. A. Self-Assembly of Self-Limiting Monodisperse Supraparticles from Polydisperse Nanoparticles. *Nat Nanotechnol.* **2011**, *6*, 580–587.
5. Cong, H. P.; Yu, S. H. Self-Assembly of Functionalized Inorganic-Organic Hybrids. *Curr. Opin. Colloid Interface Sci.* **2009**, *14*, 71–80.
6. Schedin, F.; Geim, A. K.; Morozov, S. V.; Hill, E. W.; Blake, P.; Katsnelson, M. I.; Novoselov, K. S. Detection of Individual Gas Molecules Adsorbed on Graphene. *Nat. Mater.* **2007**, *6*, 652–655.
7. Li, Y.; Wang, H.; Xie, L.; Liang, Y.; Hong, G.; Dai, H. MoS_2 Nanoparticles Grown on Graphene: An Advanced Catalyst for the Hydrogen Evolution Reaction. *J. Am. Chem. Soc.* **2011**, *133*, 7296–7299.
8. Yin, S.; Zhang, Y.; Kong, J.; Zou, C.; Li, C. M.; Lu, X.; Ma, J.; Boey, F. Y. C.; Chen, X. Assembly of Graphene Sheets into

Hierarchical Structures for High-Performance Energy Storage. *ACS Nano* **2011**, *5*, 3831–3838.
9. Chandra, V.; Park, J.; Chun, Y.; Lee, J. W.; Hwang, I.-C.; Kim, K. S. Water-Dispersible Magnetite-Reduced Graphene Oxide Composites for Arsenic Removal. *ACS Nano* **2010**, *4*, 3979–3986.
10. Zhu, Z.; Su, D.; Weinberg, G.; Schlögl, R. Supermolecular Self-Assembly of Graphene Sheets: Formation of Tube-in-Tube Nanostructures. *Nano Lett.* **2004**, *4*, 2255–2259.
11. Dikin, D. A.; Stankovich, S.; Zimney, E. J.; Piner, R. D.; Dommett, G. H. B.; Evmenenko, G.; Nguyen, S. T.; Ruoff, R. S. Preparation and Characterization of Graphene Oxide Paper. *Nature* **2007**, *448*, 457–460.
12. Tang, L.; Wang, Y.; Li, Y.; Feng, H.; Lu, J.; Li, J. Preparation, Structure, and Electrochemical Properties of Reduced Graphene Sheet Films. *Adv. Funct. Mater.* **2009**, *19*, 2782–2789.
13. Wu, Q.; Xu, Y.; Yao, Z.; Liu, A.; Shi, G. Supercapacitors Based on Flexible Graphene/Polyaniline Nanofiber Composite Films. *ACS Nano* **2010**, *4*, 1963–1970.
14. Cote, L. J.; Cruz-Silva, R.; Huang, J. Flash Reduction and Patterning of Graphite Oxide and Its Polymer Composite. *J. Am. Chem. Soc.* **2009**, *131*, 11027–11032.
15. Vickery, J. L.; Patil, A. J.; Mann, S. Fabrication of Graphene−Polymer Nanocomposites with Higher-Order Three-Dimensional Architectures. *Adv. Mater.* **2009**, *21*, 2180–2184.
16. Cai, D.; Song, M. Recent Advance in Functionalized Graphene/Polymer Nanocomposites. *J. Mater. Chem.* **2010**, *20*, 7906–7915.
17. Bryning, M. B.; Milkie, D. E.; Islam, M. F.; Hough, L. A.; Kikkawa, J. M.; Yodh, A. G. Carbon Nanotube Aerogels. *Adv. Mater.* **2007**, *19*, 661–664.
18. Kovtyukhova, N. I.; Mallouk, T. E.; Pan, L.; Dickey, E. C. Individual Single-Walled Nanotubes and Hydrogels Made by Oxidative Exfoliation of Carbon Nanotube Ropes. *J. Am. Chem. Soc.* **2003**, *125*, 9761–9769.
19. Ogoshi, T.; Takashima, Y.; Yamaguchi, H.; Harada, A. Chemically-Responsive Sol−Gel Transition of Supramolecular Single-Walled Carbon Nanotubes (SWNTs) Hydrogel Made by Hybrids of Swnts and Cyclodextrins. *J. Am. Chem. Soc.* **2007**, *129*, 4878–4879.
20. Olsson, R. T.; Samir, M.; Salazar-Alvarez, G.; Belova, L.; Strom, V.; Berglund, L. A.; Ikkala, O.; Nogues, J.; Gedde, U. W. Making Flexible Magnetic Aerogels and Stiff Magnetic Nanopaper Using Cellulose Nanofibrils as Templates. *Nat. Nanotechnol.* **2010**, *5*, 584–588.
21. Worsley, M. A.; Pauzauskie, P. J.; Olson, T. Y.; Biener, J.; Satcher, J. H.; Baumann, T. F. Synthesis of Graphene Aerogel with High Electrical Conductivity. *J. Am. Chem. Soc.* **2010**, *132*, 14067–14069.
22. Xu, Y.; Wu, Q.; Sun, Y.; Bai, H.; Shi, G. Three-Dimensional Self-Assembly of Graphene Oxide and DNA into Multifunctional Hydrogels. *ACS Nano* **2010**, *4*, 7358–7362.
23. Tang, Z.; Shen, S.; Zhuang, J.; Wang, X. Noble-Metal-Promoted Three-Dimensional Macroassembly of Single-Layered Graphene Oxide. *Angew. Chem., Int. Ed.* **2010**, *49*, 4603–4607.
24. Jiang, X.; Ma, Y. W.; Li, J. J.; Fan, Q. L.; Huang, W. Self-Assembly of Reduced Graphene Oxide into Three-Dimensional Architecture by Divalent Ion Linkage. *J. Phys. Chem. C* **2010**, *114*, 22462–22465.
25. Bai, H.; Li, C.; Wang, X.; Shi, G. On the Gelation of Graphene Oxide. *J. Phys. Chem. C* **2011**, *115*, 5545–5551.
26. Xu, Y.; Sheng, K.; Li, C.; Shi, G. Self-Assembled Graphene Hydrogel *via* a One-Step Hydrothermal Process. *ACS Nano* **2010**, *4*, 4324–4330.
27. Chen, W. F.; Yan, L. F. *In Situ* Self-Assembly of Mild Chemical Reduction Graphene for Three-Dimensional Architectures. *Nanoscale* **2011**, *3*, 3132–3137.
28. Sheng, K.-X.; Xu, Y.-X.; Li, C.; Shi, G.-Q. High-Performance Self-Assembled Graphene Hydrogels Prepared by Chemical Reduction of Graphene Oxide. *New Carbon Mater.* **2011**, *26*, 9–15.
29. Chen, S.; Zhu, J.; Wu, X.; Han, Q.; Wang, X. Graphene Oxide−MnO_2 Nanocomposites for Supercapacitors. *ACS Nano* **2010**, *4*, 2822–2830.
30. Wang, H.; Casalongue, H. S.; Liang, Y.; Dai, H. $Ni(OH)_2$ Nanoplates Grown on Graphene as Advanced Electrochemical Pseudocapacitor Materials. *J. Am. Chem. Soc.* **2010**, *132*, 7472–7477.
31. Cong, H.-P.; He, J.-J.; Lu, Y.; Yu, S.-H. Magnetic Graphene: Water-Soluble Magnetic-Functionalized Reduced Graphene Oxide Sheets: *In Situ* Synthesis and Magnetic Resonance Imaging Applications. *Small* **2010**, *6*, 169–173.
32. Chen, W.; Li, S.; Chen, C.; Yan, L. Self-Assembly and Embedding of Nanoparticles by *in Situ* Reduced Graphene for Preparation of a 3D Graphene/Nanoparticle Aerogel. *Adv. Mater.* **2011**, *23*, 5679–5683.
33. Måkie, P.; Westin, G.; Persson, P.; Österlund, L. Adsorption of Trimethyl Phosphate on Maghemite, Hematite, and Goethite Nanoparticles. *J. Phys. Chem. A* **2011**, *115*, 8948–8959.
34. Shin, H.-J.; Kim, K. K.; Benayad, A.; Yoon, S.-M.; Park, H. K.; Jung, I.-S.; Jin, M. H.; Jeong, H.-K.; Kim, J. M.; Choi, J.-Y.; Lee, Y. H. Efficient Reduction of Graphite Oxide by Sodium Borohydride and Its Effect on Electrical Conductance. *Adv. Funct. Mater.* **2009**, *19*, 1987–1992.
35. Ferrari, A. C.; Robertson, J. Interpretation of Raman Spectra of Disordered and Amorphous Carbon. *Phys. Rev. B* **2000**, *61*, 14095–14107.
36. Ban, C.; Wu, Z.; Gillaspie, D. T.; Chen, L.; Yan, Y.; Blackburn, J. L.; Dillon, A. C. Nanostructured Fe_3O_4/SWNT Electrode: Binder-Free and High-Rate Li-Ion Anode. *Adv. Mater.* **2010**, *22*, E145–E149.
37. Ni, S.; Wang, X.; Zhou, G.; Yang, F.; Wang, J.; Wang, Q.; He, D. Hydrothermal Synthesis of Fe_3O_4 Nanoparticles and Its Application in Lithium Ion Battery. *Mater. Lett.* **2009**, *63*, 2701–2703.
38. Smith, A. M.; Williams, R. J.; Tang, C.; Coppo, P.; Collins, R. F.; Turner, M. L.; Saiani, A.; Ulijn, R. V. Fmoc-Diphenylalanine Self Assembles to a Hydrogel *via* a Novel Architecture Based on Π−Π Interlocked B-Sheets. *Adv. Mater.* **2008**, *20*, 37–41.
39. Banerjee, S.; Das, R. K.; Maitra, U. Supramolecular Gels 'in Action'. *J. Mater. Chem.* **2009**, *19*, 6649–6687.
40. Gao, M.-R.; Zhang, S.-R.; Jiang, J.; Zheng, Y.-R.; Tao, D.-Q.; Yu, S.-H. One-Pot Synthesis of Hierarchical Magnetite Nanochain Assemblies with Complex Building Units and Their Application for Water Treatment. *J. Mater. Chem.* **2011**, *21*, 16888–16892.
41. Xue, Y.; Chen, H.; Yu, D.; Wang, S.; Yardeni, M.; Dai, Q.; Guo, M.; Liu, Y.; Lu, F.; Qu, J.; Dai, L. Oxidizing Metal Ions with Graphene Oxide: The in Situ Formation of Magnetic Nanoparticles on Self-Reduced Graphene Sheets for Multifunctional Applications. *Chem. Commun.* **2011**, *47*, 11689–11691.
42. Qu, Q.; Yang, S.; Feng, X. 2d Sandwich-Like Sheets of Iron Oxide Grown on Graphene as High Energy Anode Material for Supercapacitors. *Adv. Mater.* **2011**, *23*, 5574–5580.
43. Yuan, J.; Liu, X.; Akbulut, O.; Hu, J.; Suib, S. L.; Kong, J.; Stellacci, F. Superwetting Nanowire Membranes for Selective Absorption. *Nat. Nanotechnol.* **2008**, *3*, 332–336.
44. Zou, R.; Zhang, Z.; Yu, L.; Tian, Q.; Wu, J.; Sun, Y.; Chen, Z.; Hu, J. Oriented Free-Standing Ammonium Vanadium Oxide Nanobelt Membranes: Highly Selective Absorbent Materials. *Chem.—Eur. J.* **2010**, *16*, 14307–14312.
45. Shieh, J.; Hou, F. J.; Chen, Y. C.; Chen, H. M.; Yang, S. P.; Cheng, C. C.; Chen, H. L. Robust Airlike Superhydrophobic Surfaces. *Adv. Mater.* **2010**, *22*, 597–601.
46. Liang, H.-W.; Cao, X.; Zhang, W.-J.; Lin, H.-T.; Zhou, F.; Chen, L.-F.; Yu, S.-H. Robust and Highly Efficient Free-Standing Carbonaceous Nanofiber Membranes for Water Purification. *Adv. Funct. Mater.* **2011**, *21*, 3851–3858.
47. Li, H.; Li, W.; Zhang, Y.; Wang, T.; Wang, B.; Xu, W.; Jiang, L.; Song, W.; Shu, C.; Wang, C. Chrysanthemum-Like [Alpha]-FeOOH Microspheres Produced by a Simple Green Method and Their Outstanding Ability in Heavy Metal Ion Removal. *J. Mater. Chem.* **2011**, *21*, 7878–7881.
48. Langmuir, I. The Adsorption of Gases on Plane Surfaces of Glass, Mica and Platinum. *J. Am. Chem. Soc.* **1918**, *40*, 1361–1403.

49. Wang, P.; Lo, I. M. C. Synthesis of Mesoporous Magnetic γ-Fe_2O_3 and Its Application to Cr(VI) Removal from Contaminated Water. *Water Res.* **2009**, *43*, 3727–3734.
50. Babu, B.; Gupta, S. Adsorption of Cr(VI) Using Activated Neem Leaves: Kinetic Studies. *Adsorption* **2008**, *14*, 85–92.
51. Huang, Z.-H.; Zheng, X.; Lv, W.; Wang, M.; Yang, Q.-H.; Kang, F. Adsorption of Lead(II) Ions from Aqueous Solution on Low-Temperature Exfoliated Graphene Nanosheets. *Langmuir* **2011**, *27*, 7558–7562.
52. Su, D. S.; Chen, X.; Weinberg, G.; Klein-Hofmann, A.; Timpe, O.; Hamid, S. B. A.; Schlögl, R. Hierarchically Structured Carbon: Synthesis of Carbon Nanofibers Nested inside or Immobilized onto Modified Activated Carbon. *Angew. Chem., Int. Ed.* **2005**, *44*, 5488–5492.
53. Guo, X.; Chen, F. Removal of Arsenic by Bead Cellulose Loaded with Iron Oxyhydroxide from Groundwater. *Environ. Sci. Technol.* **2005**, *39*, 6808–6818.
54. Hummers, W. S.; Offeman, R. E. Preparation of Graphitic Oxide. *J. Am. Chem. Soc.* **1958**, *80*, 1339–1339.
55. Singh, R.; Misra, V.; Singh, R. Synthesis, Characterization and Role of Zero-Valent Iron Nanoparticle in Removal of Hexavalent Chromium from Chromium-Spiked Soil. *J. Nanopart. Res.* **2011**, *13*, 4063–4073.